Kinetic Simulations of the Self-Focusing and Dissipation of Finite-Width Electron Plasma Waves

B. J. Winjum,[1] R. L. Berger,[2] T. Chapman,[2] J. W. Banks,[2] and S. Brunner[3]

[1]*Department of Electrical Engineering, University of California Los Angeles, Los Angeles, California 90095, USA*
[2]*Lawrence Livermore National Laboratory, P. O. Box 808, Livermore, California 94551, USA*
[3]*Centre de Recherches en Physique des Plasmas, Association EURATOM-Confédération Suisse, Ecole Polytechnique Fédérale de Lausanne, CRPP-PPB, CH-1015 Lausanne, Switzerland*

(Received 9 June 2013; published 6 September 2013)

Two-dimensional simulations, both Vlasov and particle-in-cell, are presented that show the evolution of the field and electron distribution of finite-width, nonlinear electron plasma waves. The intrinsically intertwined effects of self-focusing and dissipation of field energy caused by electron trapping are studied in simulated systems that are hundreds of wavelengths long in the transverse direction but only one wavelength long and periodic in the propagation direction. From various initial wave states, both the width at focus Δ_m relative to the initial width Δ_0 and the maximum field amplitude at focus are shown to be a function of the growth rate of the transverse modulational instability γ_{TPMI} divided by the loss rate of field energy ν_E to electrons escaping the trapping region. With dissipation included, an amplitude threshold for self-focusing $\gamma_{\mathrm{TPMI}}/\nu_E \sim 1$ is found that supports the analysis of Rose [Phys. Plasmas **12**, 012318 (2005)].

DOI: 10.1103/PhysRevLett.111.105002 PACS numbers: 52.35.Fp, 52.35.Mw, 52.65.Ff, 52.65.Rr

The kinetic evolution of large-amplitude electron plasma waves (EPWs) continues to play a central role in fundamental theory and experiments of wave-particle interactions [1–6] as well as in inertial confinement fusion (ICF) and space plasmas. In ICF, large-amplitude EPWs reflect the laser light incident on ignition hohlraums via stimulated Raman scattering (SRS), the backscatter of an intense coherent light wave into a lower frequency light wave by an EPW. SRS is the primary laser energy loss mechanism in ICF experiments at the National Ignition Facility where, on some beams, up to 30% of the light is backscattered [7–9]. In space plasmas, the stability of large-amplitude EPWs excited via two-stream instabilities with a class of trapped electron distributions referred to as electron phase space holes is of great interest [10–12].

In laser-driven ICF, EPWs are driven predominantly in spatially localized laser speckles with approximate width given by the f/number of the focusing optics ($f/8$ for the National Ignition Facility) times the laser wavelength (351 nm) and thus are transversely localized by the excitation process. As proposed by Rose [4,13], these finite-width EPWs can self-focus due to the trapped particle modulational instability (TPMI) with growth rate γ_{TPMI}. With particle-in-cell (PIC) simulations, several authors have studied SRS in finite-width laser speckles and have found structure consistent with kinetic self-focusing of EPWs [14–17]. However, in these studies, the myriad of physical processes at play can mask the essential features of EPW evolution and make scaling studies nigh impossible. More carefully controlled simulations of finite-width EPWs with an external driver have been performed with Vlasov [18] as well as PIC [19] codes. Whereas the PIC studies [19] found that the physical process dominating the transverse evolution of the EPW was local damping of the EPWs at the transverse edge by transiting electrons, the Vlasov studies [18] found that the EPWs self-focused, provided the wave amplitude and transverse width were large enough.

The single process of electron trapping and detrapping in a finite-width EPW leads to both self-focusing and loss of field energy. We show in this Letter that the condition $\gamma_{\mathrm{TPMI}}/\nu_E \sim 1$, where ν_E is the field energy dissipation rate, sets a threshold for EPW self-focusing in qualitative agreement with Ref. [4]. The self-focusing leads to an increase of EPW amplitude on axis as the EPW narrows transversely. The phase space evolution of trapped and detrapped electrons as the EPW narrows clearly illustrates the energy loss dynamics. We find that the loss rate $\nu_E \propto \nu_{\mathrm{sl}}$, where the side loss rate $\nu_{\mathrm{sl}} = \tau_{\mathrm{sl}}^{-1} = v_e/\Delta_0$, Δ_0 is the FWHM of the external driver field intensity, and $v_e = \sqrt{T_e/m_e}$ is the electron thermal velocity with T_e (m_e) the electron temperature (mass).

Both PIC and Vlasov codes are used to study externally driven, two-dimensional (2D) EPWs with $k\lambda_{\mathrm{De}} = 1/3$, a value typical for EPWs driven by SRS [7–9]; here, $k = 2\pi/\lambda_0$ and λ_0 are, respectively, the EPW wave number and wavelength along the propagation direction x and $\lambda_{\mathrm{De}} = v_e/\omega_{\mathrm{pe}}$ is the electron Debye length with ω_{pe} the electron plasma frequency. The driver frequency $\omega_0 \approx 1.2\omega_{\mathrm{pe}}$ is chosen to satisfy the linear kinetic dispersion relation, with the resulting EPW phase velocity $v_p \approx 3.6v_e$. The linear Landau damping rate $\nu_0 = 0.026\omega_{\mathrm{pe}}$ is an order of magnitude larger than the rate at which we find the field energy to decay. Note that Refs. [20,21] showed that the dominant detrapping mechanism for EPWs localized in laser speckles is side loss, not collisions, justifying our

use of collisionless simulations. We furthermore neglect ion dynamics, since TPMI is faster than processes such as ponderomotive self-focusing that require ions.

The PIC simulations were done with the 2D electrostatic PIC code BEPS, based on the UCLA parallel particle-in-cell (UPIC) framework [22]; the 2D Vlasov simulations used LOKI [23]. The two independent techniques give added confidence in the results: PIC simulations have a long history in simulating these processes, while Vlasov codes with no statistical noise allow clearer simulation of smaller wave amplitudes. The system length $L_x = \lambda_0$ along x. The BEPS and LOKI boundary conditions for electrostatic fields were periodic in all directions. The boundary conditions were periodic for the LOKI distribution function and the BEPS electrons in x. At the lateral boundaries in LOKI, outgoing boundary conditions were applied; BEPS used wide enough lateral simulation domains that the periodic boundary conditions did not affect the wave evolution. BEPS simulations used 16 384 particles per cell; LOKI's typical maximum velocity was 7–8v_e. We normalize distance to $\lambda_{\rm De}$ and electric fields to $T_e/(e\lambda_{\rm De})$.

Traveling waves with approximately Gaussian transverse profile were excited via an externally imposed electric field whose amplitude remained constant for $\omega_{\rm pe}t = 100$ with rise and fall times of one wave period [24]. The waves were driven to potential amplitudes ranging over $10^{-3} < e\phi_0/T_e < 1$, where the subscript 0 denotes the maximum amplitude of the EPW reached at time t_0 near when the driver was turned off. Using the electron bounce frequency, given by $\omega_{\rm be} = k\sqrt{e\phi_0/m_e}$, we find the approximate number of bounce periods $\omega_{\rm be}t_0/2\pi \lesssim 5$ for all amplitudes considered. Thus, one might expect the distribution and the frequency shift to be in the sudden limit [21,25,26], although the actual distributions in Vlasov simulations often are closer to the adiabatic limit. In our interpretation of the simulation results, we take the nonlinear frequency shift from trapped electrons $\delta\omega/\omega_{\rm pe} = -0.04\sqrt{e\phi_0/T_e}$, a value close to the adiabatic one.

In all simulations, the waves were driven to large enough amplitudes to exceed the bounce number threshold $N_b = (\Delta_0/\lambda_{\rm De})\sqrt{e\phi_0/T_e}(k\lambda_{\rm De}/2\pi)$, established in Ref. [20], for the wave to trap electrons and modify the dispersion and damping rate [27]. We chose EPW driver widths in the range $\Delta_0 \sim 100$–$600\lambda_{\rm De}$ based on the typical laser speckle width, which is many Debye lengths wide: $f\lambda_L/\lambda_{\rm De} = 142f\sqrt{N_e/(N_c T_{e,\rm keV})} \sim 360$ for $f = 8$, $T_{e,\rm keV} = 1$, $\lambda_L = 351$ nm is the laser wavelength, and $N_e/N_c = 0.1$, where N_e is the electron density and N_c is the critical density. Similarly to N_b, the threshold parameter shown in this Letter $\gamma_{\rm TPMI}/\nu_E \propto \Delta_0\sqrt{\phi_0}$; both are a measure of trapping versus detrapping rates.

A characteristic example of the wave evolution is shown in Fig. 1 for a wave with $e\phi_0/T_e = 0.21$ and width Δ (field intensity FWHM) at t_0 of $\Delta_0 = 532\lambda_{\rm De}$. Figure 1(a) shows the wave as the driver is turning off with nearly planar wave fronts. At $\omega_{\rm pe}t = 1000$, the wave fronts shown in Fig. 1(b) are clearly bowed and the focusing has begun even though the maximum wave amplitude has not increased. At $\omega_{\rm pe}t = 1800$, shown in Fig. 1(c), the wave is nearing its minimum width and its maximum amplitude. Subsequently, the wave diffracts and the wave amplitude decreases. Figure 1(d) shows the maximum amplitude on axis ($y = 0$) as a function of time. The maximum is reached at $t_m \approx 1800/\omega_{\rm pe}$; we denote the width at t_m as Δ_m.

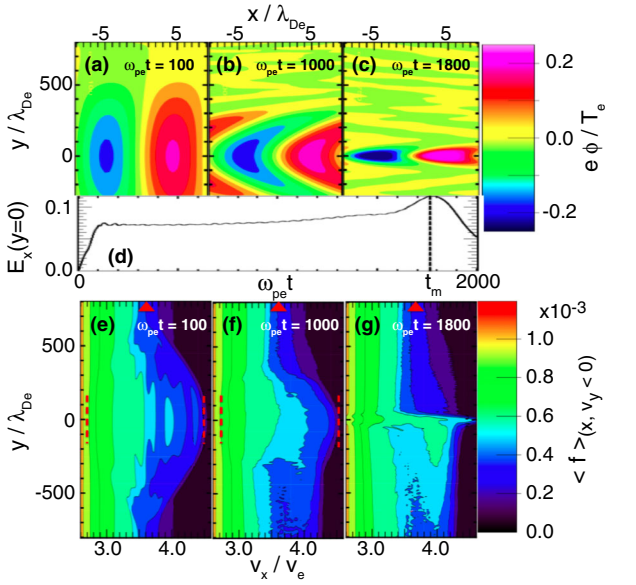

FIG. 1 (color online). Snapshots of the rightward propagating wave potential $\phi(x, y)$ for the LOKI simulation with $e\phi_0/T_e = 0.21$ and $\Delta_0 = 532\lambda_{\rm De}$ at the times (a) $\omega_{\rm pe}t = 100$, (b) 1000, and (c) 1800. The field is symmetric about $y = 0$. In (d), the time evolution of the maximum field E_x, which reaches a maximum at $\omega_{\rm pe}t_m = 1800$, is shown. In (e)–(g), snapshots at $\omega_{\rm pe}t = 100$, 1000, and 1800, respectively, are shown of the distribution as a function of $y/\lambda_{\rm De}$ and $2.6 < v_x/v_e < 4.6$; the distribution is averaged over x and all $v_y < 0$. The phase velocity $= 3.6v_e$ is indicated by the red triangles. The dashed red lines show the edge of the trapping region in v_x at $v_p \pm 2\sqrt{e\phi_{\rm max}/m_e}$.

Also shown in Figs. 1(e)–1(g) is the evolution of the distribution of electrons that interact with the field at times corresponding to snapshots of the field in Figs. 1(a)–1(c). The distribution has been integrated over x and $v_y < 0$ in order to highlight key features, hence the apparent asymmetry in y. Electrons are introduced at the boundary $y = +L_y$ with a Maxwell-Boltzmann distribution. Figures 1(e)–1(g) reveal how electrons enter the wave transversely, gain energy as they become trapped in x while advecting on average at v_e, and then exit transversely with a non-Maxwell-Boltzmann distribution in v_x. The exiting distribution has more energy than the entering one, which results in a field energy loss rate ν_E. This process, which is

accentuated as the field focuses transversely, limits the amplitude of the field on axis.

A number of authors [4,13,18,28] have modeled EPWs with an enveloped nonlinear Schrödinger equation. From the EPW dispersion relation and with the eikonal expansion $\phi = (1/2)\tilde{\phi}\exp(-i\omega_0 t + ik_0 x) + \text{c.c.}$, one obtains

$$(\partial_t + v_g\partial_x - iD_x\partial_x^2 - iD_\perp\partial_y^2 + i\delta\omega + \nu)\tilde{\phi} = \alpha\phi_d(y,t), \quad (1)$$

where $\partial_j^n \equiv \partial^n/\partial j^n$, $\tilde{\phi}$ is a slowly varying envelope, v_g is the group velocity, $\delta\omega$ is an amplitude-dependent, negative frequency shift [25,26], ν is a heuristic damping term, ϕ_d is the driving potential, α is a coupling constant, and (for the Bohm-Gross dispersion relation and the kinetic EPW dispersion) D_x and $D_\perp$ are positive. Coupling to harmonics is assumed negligible as they play an insignificant role in the simulations.

We chose to study transverse phenomena without the modulational sideband instability [29,30] by choosing $L_x = \lambda_0$. With that restriction, $\partial_x\tilde{\phi} = 0$. Then, as shown by Rose [4,13], one finds a transverse modulational or self-focusing instability with maximum growth rate $\gamma_{\text{TPMI}} = |\delta\omega|/4$, provided $D_\perp\delta\omega < 0$. With $\nu > 0$ to account for the loss of field energy to escaping trapped electrons, linear stability analysis finds growth only above the threshold $\gamma_{\text{TPMI}} > \nu$. Solving Eq. (1) with $\partial_x\tilde{\phi} = 0$ and $\nu = 0$, we find similar behavior to Fig. 1(d) but with the maximum value of E_x ~4× its initial value, whereas the field on axis in the simulation [Fig. 1(c)] is only ~1.5× larger, clearly illustrating the significant effect of damping. Correspondingly, $\Delta_m/\Delta_0 = 0.03$ is narrower in the model equation without damping compared to $\Delta_m/\Delta_0 = 0.09$ in the simulation. Unlike ponderomotive self-focusing, here the resonant wave-particle interaction leads both to a focusing via a transversely varying frequency shift $\delta\omega$ and to a loss rate $\nu = \nu_E$.

To quantify the effect of dissipation on the EPWs, we measure the rate that the total field energy decays as the escaping electrons take energy away. Figure 2(a) shows the time history of the total field energy for two LOKI simulations: one just above the threshold for self-focusing and one just below. There are two phases to the loss rate. The early rate ν_E decreases as a function of increasing initial field amplitude; the late rate is much faster. For amplitudes far below threshold, there is one fast rate. The rates were determined by fitting to an exponential decay as shown by the examples in Fig. 2(a) by the blue and green lines.

Reference [18] showed that the field energy decreased with time at a rate proportional to the side loss rate $\nu_{\text{sl}} = v_e/\Delta_0$. The damping rate ν_E normalized to ν_{sl} is plotted as a function of $e\phi_0/T_e$ in Fig. 2(b). Results for several Δ_0 are shown. The decay rates for the early phase ν_E are proportional to $\nu_{\text{sl}} = \tau_{\text{sl}}^{-1}$ with a jump in value at $e\phi_0/T_e \gtrsim 0.01$. Note that above $e\phi_0/T_e \simeq 0.01$, the

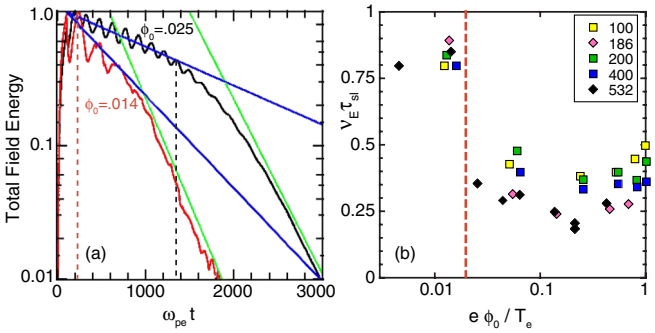

FIG. 2 (color online). (a) For $\Delta_0 = 532\lambda_{\text{De}}$, the temporal evolution of total field energy (normalized to the maximum value) is shown for $e\phi_0/T_e = 0.025$ ($\gamma_{\text{TPMI}}/\nu_E = 2.35$) and $e\phi_0/T_e = 0.014$ ($\gamma_{\text{TPMI}}/\nu_E = 0.74$). Exponential fits are shown to the early and late decays by the blue and green lines, respectively. Vertical dashed black and red lines indicate t_m for $e\phi_0/T_e = 0.025$ and $e\phi_0/T_e = 0.014$, respectively. (b) The energy loss rate ν_E normalized to the side loss time τ_{sl} for several initial FWHM widths Δ_0/λ_{De}. Diamond and square markers denote LOKI and BEPS simulations, respectively. The vertical dashed line indicates the threshold value of $e\phi_0/T_e$.

BEPS rates are larger (by at most a factor of 2) than the LOKI rates.

To illustrate the time evolution of the EPW width, we compute $\bar{E}^2(y,t) = L_x^{-1}\int_0^{L_x} dx|E_x(x,y,t)|^2$. Figure 3 shows $\bar{E}^2(y,t)$ for simulations with two different initial amplitudes. Figure 3(a) shows an EPW that damps and transversely localizes before self-focusing affects the wave profile. Figure 3(b) is sufficiently wide and intense to reach a narrow focus limited by diffraction and side loss at t_m, after which the field energy is rapidly depleted. By

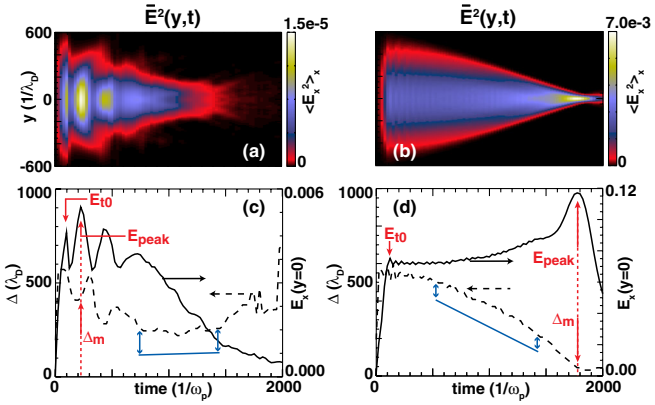

FIG. 3 (color online). $\bar{E}^2(y,t)$ for $\Delta_0 = 532\lambda_{\text{De}}$ and (a) $e\phi_0/T_e \approx 0.014$ (b) $e\phi_0/T_e \approx 0.21$. (b) From the LOKI simulation shown in Fig. 1. In (c) and (d), the time dependence of the maximum field on axis (solid line and right-hand-side axis) and Δ (dashed line and left-hand-side axis) are shown for the same conditions as in (a) and (b), respectively. The blue lines in (c) and (d) show the linear fit to Δ used to determine the localization velocity V_l.

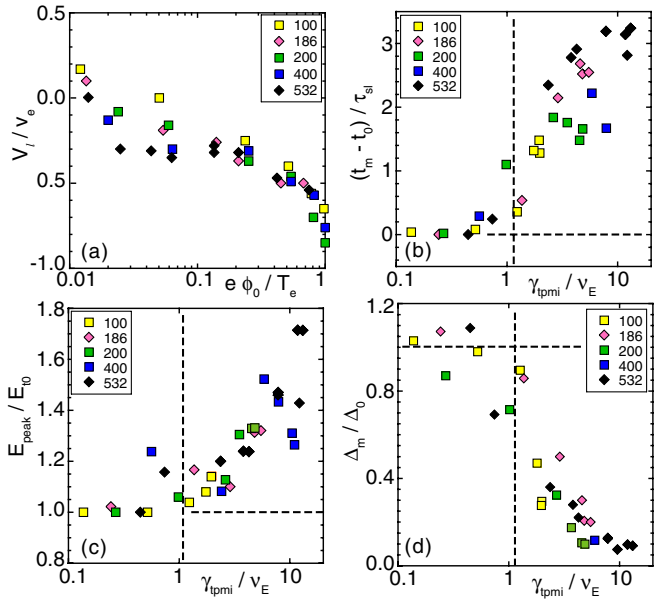

FIG. 4 (color online). (a) Localization velocity versus wave amplitude $e\phi_0/T_e$ for several initial FWHM widths Δ_0/λ_{De}. (b) The relative time $(t_m - t_0)/\tau_{sl}$, (c) the peak $E_x(y = 0)$ over all time divided by E_{t_0}, and (d) Δ_m/Δ_0, all as a function of γ_{TPMI}/ν_E. Diamond markers are LOKI simulations; square markers are BEPS simulations. The vertical dashed lines in (b)–(d) indicate the threshold value of γ_{TPMI}/ν_E. The horizontal dashed lines indicate the expected values below threshold.

assuming that $\Delta = \Delta_{t_1} + V_l(t - t_1)$, we compute the localization velocity V_l/v_e, where t_1 is a time several bounce times after the drive is turned off and before t_m.

Figure 4(a) shows the dependence of V_l on $e\phi_0/T_e$ for a variety of initial EPW widths Δ_0. For low amplitudes, V_l depends on Δ_0, which indicates that diffraction is important for the narrower widths [18]. For high amplitudes, V_l is independent of Δ_0 and approaches the electron thermal velocity in magnitude. That is, an untrapped electron needs a significant transverse velocity to become trapped. On the other hand, trapped electrons are detrapped more quickly than the side loss rate would predict. We also found that V_l is sensitive to $k\lambda_{De}$ (not shown). However, the ratio of V_l/v_e to $\gamma_{TPMI}/\omega_{pe}$ as a function of $e\phi_0/T_e$ is approximately constant for different $k\lambda_{De}$; this scaling of the localization velocity applies at least over the range $0.25 < k\lambda_{De} < 0.4$.

We define a threshold parameter γ_{TPMI}/ν_E calculated using ν_E from Fig. 2(b). Three important features of EPW self-focusing are shown to be a function of this parameter: the time that the field achieves its maximum value on axis (t_m), the peak value of the maximum field on axis (E_{peak}), and the width of the field intensity (Δ_m) at t_m. Figures 4(b)–4(d) show that these quantities, normalized and scaled, are nearly independent of Δ_0 and depend only on the value of the threshold parameter γ_{TPMI}/ν_E. Plotted against γ_{TPMI}/ν_E, one sees that $t_m - t_0$ jumps above 0 when the self-focusing threshold is exceeded, that is, $\gamma_{TPMI}/\nu_E \gtrsim 1$. Figure 4(c) shows how E_{peak} increases above E_{t0} as a function of γ_{TPMI}/ν_E. Below threshold, the field on axis after a bounce period or two only decreases after the drive is turned off. Figure 4(d) shows that the EPW narrows to a relative width Δ_m/Δ_0 at t_m that is independent of Δ_0 and scales as one expects from an instability; that is, it has a threshold and reaches a limit determined in this case by diffraction and side loss. For all cases considered, E_{peak} has a smaller value with a larger width Δ_m at focus which occurs at an earlier time t_m in the simulation than in the model Eq. (1) with $\nu = 0$. Below and near threshold, EPWs with smaller Δ_0 localize less proportionately. This might be expected because, as noted in Ref. [18], diffraction opposes localization and the electron distribution in the trapping region tries to evolve to a more uniform distribution transversely as the electrons travel laterally. These effects are less important for bigger Δ_0.

The LOKI and BEPS results are in substantial agreement. The differences are currently under investigation. For example, the reader may notice from Fig. 4(a) that the BEPS simulations extend to larger initial wave amplitudes ϕ_0 and thus extend to larger γ_{TPMI}. Nonetheless, the LOKI simulations achieve larger values of the parameter γ_{TPMI}/ν_E in Figs. 4(b)–4(d) because of the smaller value of ν_E as shown in Fig. 2(b). Note also that E_{peak} achieves larger values at later times t_m in LOKI than in BEPS simulations. That behavior is also consistent with solutions of Eq. (1) with smaller damping rates. In part, the differences also arise from growth of filaments from the larger initial transverse nonuniformities in BEPS which can cause the field to break into multiple foci at large amplitude, thus limiting the peak amplitude achievable in a single focus. The most physical result depends on the actual physical EPW initial fluctuation levels which neither simulation method attempts to address in this Letter.

For $\gamma_{TPMI}/\nu_E > 1$, the overall effect on SRS should be to spatially limit the backscatter to a smaller fraction of the incident light power than a fluid simulation, since the maximum wave amplitude is limited to small increases while the transverse size decreases substantially. Thus, the overlap of the speckle-wide light waves and the narrower EPWs in space is reduced.

We have presented two-dimensional kinetic simulations showing the self-focusing and dissipation of finite-width, nonlinear EPWs. We measured the rate at which the transverse wave envelope decreases in width (the transverse localization velocity) and the rate at which the total field energy decreases. The threshold for the onset of self-focusing was shown to depend on γ_{TPMI}/ν_E, in agreement with Rose [4]. The dispersion relation for EPWs in Ref. [4] assumes that phase matching is maintained with the light waves. As a consequence, Ref. [4] also predicts stability for $k\lambda_{De} > 0.46$ and stability for even lower values of $k\lambda_{De}$ as the wave amplitude $e\phi_0/T_e$ increases. In our

simulations with the free wave dispersion for EPWs, we find neither a stability region for $k\lambda_{De} > 0.46$ nor a second stability region for large $e\phi_0/T_e$.

We are pleased to acknowledge the insight provided throughout this work by Bruce I. Cohen, Warren B. Mori, and Viktor K. Decyk. This work was performed under the auspices of the U.S. Department of Energy by the Lawrence Livermore National Laboratory under Contract No. DE-AC52-07NA27344 and funded by the Laboratory Research and Development Program at LLNL under Project Tracking Code No. 12-ERD-061. This work was also supported in part under Grants No. DE-NA0001833 and No. NSF-PHY-0904039. BEPS simulations were performed on the UCLA Hoffman2 and Dawson2 Clusters and NERSC's Hopper.

[1] T. M. O'Neil, Phys. Fluids **8**, 2255 (1965).
[2] J. H. Malmberg and C. B. Wharton, Phys. Rev. Lett. **19**, 775 (1967).
[3] J. L. Kline, D. S. Montgomery, B. Bezzerides, J. A. Cobble, D. F. DuBois, R. P. Johnson, H. A. Rose, L. Yin, and H. X. Vu, Phys. Rev. Lett. **94**, 175003 (2005).
[4] H. A. Rose, Phys. Plasmas **12**, 012318 (2005).
[5] I. Y. Dodin and N. J. Fisch, Phys. Plasmas **19**, 012102 (2012).
[6] D. Benisti, O. Morice, L. Gremillet, E. Siminos, and D. J. Strozzi, Phys. Rev. Lett. **105**, 015001 (2010).
[7] J. D. Moody, P. Michel, L. Divol, R. L. Berger *et al.*, Nat. Phys. **8**, 344 (2012).
[8] J. L. Kline, D. A. Callahan, S. H. Glenzer, N. B. Meezan, J. D. Moody *et al.*, Phys. Plasmas **20**, 056314 (2013).
[9] J. D. Moody, D. J. Strozzi, L. Divol, P. Michel *et al.*, Phys. Rev. Lett. **111**, 025001 (2013).
[10] L. Muschietti, I. Roth, C. W. Carlson, and R. E. Ergun, Phys. Rev. Lett. **85**, 94 (2000).
[11] M. V. Goldman, M. M. Oppenheim, and D. L. Newman, Geophys. Res. Lett. **26**, 1821 (1999).
[12] A. Mangeney, C. Salem, C. Lacombe, J.-L. Bougeret, C. Perche, R. Manning, P. J. Kellogg, K. Goetz, S. J. Monson, and J.-M. Bosqued, Ann. Geophys. **17**, 307 (1999).
[13] H. A. Rose and L. Yin, Phys. Plasmas **15**, 042311 (2008).
[14] L. Yin, B. J. Albright, K. J. Bowers, W. Daughton, and H. A. Rose, Phys. Rev. Lett. **99**, 265004 (2007).
[15] L. Yin, B. J. Albright, K. J. Bowers, W. Daughton, and H. A. Rose, Phys. Plasmas **15**, 013109 (2008).
[16] P. E. Masson-Laborde, W. Rozmus, Z. Peng, D. Pesme, S. Hüller, M. Casanova, V. Yu. Bychenkov, T. Chapman, and P. Loiseau, Phys. Plasmas **17**, 092704 (2010).
[17] L. Yin, B. J. Albright, H. A. Rose, D. S. Montgomery, J. L. Kline, R. K. Kirkwood, P. Michel, K. J. Bowers, and B. Bergen, Phys. Plasmas **20**, 012702 (2013).
[18] J. W. Banks, R. L. Berger, S. Brunner, B. I. Cohen, and J. A. F. Hittinger, Phys. Plasmas **18**, 052102 (2011).
[19] J. E. Fahlen, B. J. Winjum, T. Grismayer, and W. B. Mori, Phys. Rev. E **83**, 045401(R) (2011).
[20] D. J. Strozzi, E. A. Williams, H. A. Rose, D. E. Hinkel, A. B. Langdon, and J. W. Banks, Phys. Plasmas **19**, 112306 (2012).
[21] R. L. Berger, S. Brunner, T. Chapman, L. Divol, C. H. Still, and E. J. Valeo, Phys. Plasmas **20**, 032107 (2013).
[22] V. K. Decyk, Comput. Phys. Commun. **177**, 95 (2007).
[23] J. W. Banks and J. A. F. Hittinger, IEEE Trans. Plasma Sci. **38**, 2198 (2010).
[24] The transverse profile of the external driver in BEPS was $\exp[-(y/\Delta y)^2/2]$ and in LOKI was $\cos^2[2\pi y/(10\Delta y)]$ for $|y| < (10\Delta y)/4$ and 0 otherwise, with $\Delta_0 \approx 2\sqrt{\ln(2)}\Delta y$.
[25] G. J. Morales and T. M. O'Neil, Phys. Rev. Lett. **28**, 417 (1972).
[26] R. L. Dewar, Phys. Fluids **15**, 712 (1972).
[27] This number ranged from a low of 1 for the narrowest width and lowest amplitude to ~60 for the highest amplitude and widest width.
[28] R. L. Dewar, W. L. Kruer, and W. M. Manheimer, Phys. Rev. Lett. **28**, 215 (1972).
[29] W. L. Kruer, J. M. Dawson, and R. N. Sudan, Phys. Rev. Lett. **23**, 838 (1969).
[30] S. Brunner and E. J. Valeo, Phys. Rev. Lett. **93**, 145003 (2004).